Efficient silicon recycling in summer in both the Polar Frontal and Subantarctic Zones of the Southern Ocean

François Fripiat, Karine Leblanc, Marc Elskens, Anne-Julie Cavagna, Leanne Armand, Luc André, Frank Dehairs, Damien Cardinal

Vol. 435: 47–61, 2011
doi: 10.3354/meps09237

MARINE ECOLOGY PROGRESS SERIES
Mar Ecol Prog Ser

Published August 22

Efficient silicon recycling in summer in both the Polar Frontal and Subantarctic Zones of the Southern Ocean

François Fripiat[1,2,*], Karine Leblanc[3], Marc Elskens[4], Anne-Julie Cavagna[4], Leanne Armand[5], Luc André[1], Frank Dehairs[4], Damien Cardinal[1,6]

[1]Geology and Mineralogy, Section of Mineralogy and Petrography, Royal Museum for Central Africa, 3080 Tervuren, Belgium

[2]Department of Earth and Environmental Sciences, Université Libre de Bruxelles, 1050 Brussels, Belgium

[3]Aix-Marseille Université (CNRS – LOPB), UMR 6535, Laboratoire d'Océanographie Physique et Biogéochimique, OSU/Centre d'Océanologie de Marseille, 13288 Marseille Cedex 09, France

[4]Earth System Sciences & Analytical and Environmental Chemistry, Vrije Universiteit Brussel, 1050 Brussels, Belgium

[5]Department of Biological Sciences, Faculty of Science, Macquarie University, New South Wales 2109, Australia

[6]*Present address:* Laboratoire d'Océanographie et du Climat: Expérimentations et Approches Numériques, Université Pierre & Marie Curie, 75252 Paris Cedex 05, France

ABSTRACT: We measured biogenic silica ($bSiO_2$) dissolution and production rates at 3 Southern Ocean sites with contrasting biogeochemical regimes (SAZ-Sense cruise, January to February 2007). Two sites were located in the Subantarctic Zone (SAZ) southeast and southwest of Tasmania, and 1 site was in the Polar Frontal Zone (PFZ). The measurements were repeated 3 times within a time frame of 4 to 7 d. In the PFZ and the western SAZ, the release of silicon from dissolving $bSiO_2$, following a productive period, appeared sufficient to entirely sustain Si demand in surface waters. Biogenic silica dissolution was more efficient in the SAZ, likely owing to stronger microzooplankton grazing and bacterial activity. The degree of iron co-limitation correlated to $bSiO_2$ growth rates (V_{Si}, d^{-1}). Highest rates were observed in the SAZ, southeast of Tasmania, a region influenced by iron-enriched East Australian Current water advecting through the Subtropical Front. The diatom communities appeared differently adapted and conditioned, in terms of uptake ability, for growth under low $Si(OH)_4$ availability. Combining our results with existing $bSiO_2$ dissolution and production data, we estimate a spring to summer net $bSiO_2$ production for the circumpolar SAZ and PFZ regions of 7.4 and 3.6 Tmol yr^{-1}, respectively, representing 4.3 and 2.1% of the global net $bSiO_2$ production for each region. Furthermore, a clear seasonal pattern emerges with (1) higher $bSiO_2$ production in spring (0.9 to 12.7 and 6.8 to 60.7 mmol Si m^{-2} d^{-1} for the SAZ and PFZ, respectively) compared to summer (0.1 to 6.6 and 0.3 to 9.1 mmol Si m^{-2} d^{-1} for the SAZ and PFZ, respectively) and (2) a $bSiO_2$ dissolution to production ratio of <1 in spring (~0.4) and generally >1 in summer (~1.7).

KEY WORDS: Diatoms · Biogenic silica · Silicon cycle · Dissolution · Production · Southern Ocean

INTRODUCTION

Diatoms, eukaryotic unicellular microalgae with cell walls made of a composite of organic material and silica (i.e. biogenic silica, $bSiO_2$), are an ecologically significant group since they (1) account for ~40% of the upper ocean biological carbon pump (Buesseler 1998, Jin et al. 2006, Hildebrand 2008) and (2) control the oceanic silicon cycle through $bSiO_2$ production (P) and dissolution (D) in surface waters (Tréguer et al. 1995). The relative importance of these 2 processes (D:P) regulates the ability of the system to export $bSiO_2$, thereby stripping silicic acid ($Si[OH]_4$) from the surface ocean and defining the silica pump efficiency, which in turn affects global biogeochemistry (Sarmiento et al. 2004). The variability of D:P in the surface ocean is large, with values ranging from as low as 0.1 to >1.0 (Nelson et al. 1995, Brzezinski et al. 2003, Beucher et al. 2004). This

*Email: ffripiat@ulb.ac.be

range suggests that silica recycling in the surface ocean is variable, which must impact on the efficiency of the silica pump. Brzezinski et al. (2003) suggested that there is a shift in the silicon cycle mode. Dissolution of $bSiO_2$ supports either a small fraction of the gross $bSiO_2$ production during diatom blooms (i.e. efficient silica pump), or most of the gross $bSiO_2$ production during non-bloom periods (i.e. inefficient silica pump). Direct measurements of $bSiO_2$ dissolution rates are scarce for the ocean (some 57 individual profiles to date; Ragueneau et al. 2000, Brzezinski et al. 2003, Beucher et al. 2004), mainly because the methodologies used were time consuming (Nelson & Goering 1977a, Corvaisier et al. 2005). This has led to poor knowledge of the processes driving $bSiO_2$ dissolution.

The effect of the efficiency of the biological pump (C, Si, N, P, ...) on global biogeochemistry is especially pronounced in the Southern Ocean (Sarmiento et al. 2004, Sigman et al. 2010). Regarding the silicon cycle, much more attention has been given to the southern Antarctic Circumpolar Current where the bulk of the $bSiO_2$ production occurs (see e.g. Pondaven et al. 2000, Brzezinski et al. 2001, Jin et al. 2006). However, the northern part of the Antarctic Circumpolar Current (including the Polar Frontal Zone [PFZ] and Subantarctic Zone [SAZ]) is of prime importance regarding the occurrence of nutrient leakage to lower latitudes (Sarmiento et al. 2004). The efficiency of the silica pump in the PFZ and SAZ directly affects the potential of the nutrient-advecting intermediate water masses to fertilize low-latitude thermocline waters. The $bSiO_2$ production and dissolution rates vary widely; ranging from 0.2 to 60.7 and 0.2 to 5.8 mmol Si m^{-2} d^{-1}, respectively, in the PFZ and from 0.0 to 3.05 and 0.4 to 5.2 mmol Si m^{-2} d^{-1}, respectively, in the SAZ (Nelson & Gordon 1982, Brzezinski et al. 2001, Quéguiner 2001, Quéguiner & Brzezinski 2002, Leblanc et al. 2002, Beucher et al. 2004). Up until now, results for only 4 $bSiO_2$ dissolution profiles have been published for the SAZ, and 6, for the PFZ (Nelson & Gordon 1982, Brzezinski et al. 2001, Beucher et al. 2004). A better assessment of the variability of these production and dissolution rates is required to quantify (1) the impact of these areas on the global silicon budget and (2) the strength of the silicate pump in these regions.

The present study assessed summer $bSiO_2$ production (both by ^{30}Si and ^{32}Si) and dissolution (^{30}Si) in 3 biogeochemically contrasting environments of the SAZ and PFZ, south of Tasmania. The SAZ-Sense cruise objectives were to understand the mechanisms driving the observed zonal variability in chlorophyll biomass within the SAZ and between the SAZ and the PFZ (Bowie et al. 2011a). During the SAZ-Sense study it was shown by Herraiz-Borreguero & Rintoul (2011) that this variability was driven by the Tasman Outflow and the East Australian Current (EAC) affecting the eastern SAZ. Through migrating eddies, interleaving at the Subtropical Front, the EAC provided the input of warm and salty subtropical waters that were also Fe enriched (Bowie et al. 2009, Lannuzel et al. 2011, Mongin et al. 2011). In contrast, in the western SAZ, regional circulation was dominated by northwestward circulation and a deep-reaching anticyclonic recirculation, with cooler and fresher waters resulting (Herraiz-Borreguero & Rintoul 2011). Despite this fertilization and the resulting higher chlorophyll *a* (chl *a*) concentrations, in summer the eastern SAZ region was only marginally more productive (Cavagna et al. 2011) and exported less particulate carbon (Jacquet et al. 2011) than the western SAZ and PFZ regions, which both exhibited lower biomasses.

MATERIALS AND METHODS

Oceanographic settings and sampling strategy. The SAZ-Sense cruise track (21 January to 19 February 2007, RV 'Aurora Australis') followed a diamond-shaped grid in the Australian sector of the Southern Ocean, south of Tasmania (Fig. 1). Three process stations were selected on the basis of their contrasting hydrodynamics, physico-chemical and ecosystem characteristics. The objective was to occupy a station for 6 to 8 d to conduct process studies with incubation experiments and to replicate sampling over several days. Process Station 1 (P1, 46.3° S, 140.6° E; 22 to 29 January 2007) was located in northwestern SAZ waters, Process Station 2 (P2, 54.0° S, 145.9° E; 1 to 6 February 2007) was in the PFZ, and Process Station 3 (P3, 45.5° S, 153.2° E; 10 to 15 February 2007) was located in a highly dynamic region at the northernmost edge of the eastern SAZ. P3 was enriched in iron (Lannuzel et al. 2011). These observations agreed well with simulated iron supply (Mongin et al. in press), which indicated that increased iron concentrations at P3 were due to both seasonal delivery from southward advection of iron-rich subtropical waters (driven by the EAC) and to the dissolution of trace elements from wind-blown dust deposition off the Australian continent (Bowie et al. 2011a).

^{30}Si incubations were performed at process stations on 3 different days to cover short-term temporal variability. ^{32}Si incubations were performed simultaneously (same CTD casts) with short-term ^{13}C and ^{15}N incubations (Cavagna et al. 2011) and bacterial production/activity measurements (Dumont et al. 2011). Rates were determined at 4 depths corresponding to 100, 50, 25 and 1% of PAR (photosynthetic active radiation) light depths. Polycarbonate incubation bottles (4 l) were wrapped in neutral-density screens simula-

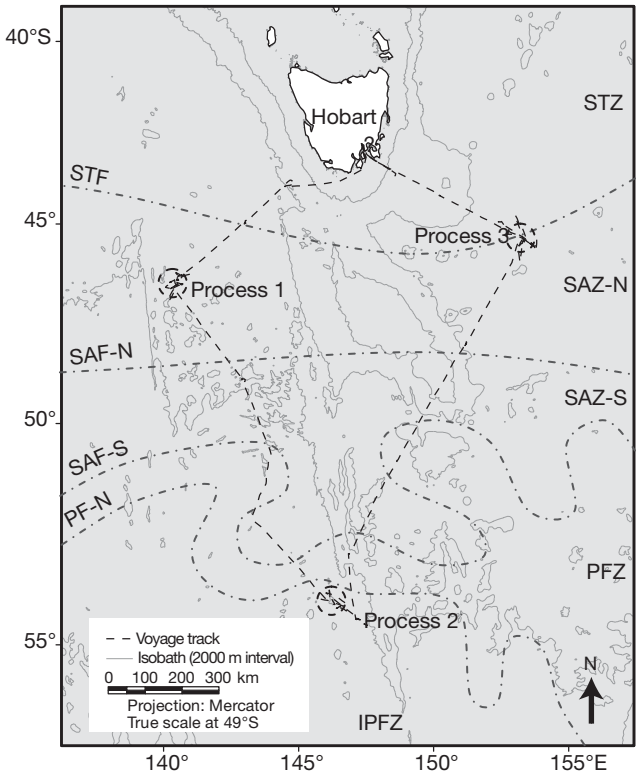

Fig. 1. SAZ-Sense voyage track (dashed line) and station locations (from de Salas et al. 2011). STZ: Subtropical Zone; STF: Subtropical Front; SAZ-N: Northern Subantarctic Zone; SAF-N: North Subantarctic Front; SAZ-S: Southern Subantarctic Zone; SAF-S: South Subantarctic Front; PFZ: Polar Frontal Zone; PF-N: North Polar Front; IPFZ: Inter-Polar-Frontal Zone; dot-dashed lines are the fronts

ting incoming irradiance and were incubated for 24 h (t24) and 48 h (t48) at local surface water temperature in a flow-through, on-deck incubator.

Production and dissolution rates of $bSiO_2$. Seawater was spiked with ^{30}Si-enriched solution (99.62%, Chemgas; Nelson & Goering 1977a,b). The production rate of $bSiO_2$ was assessed from the change in isotopic composition of the particulate phase (increase in ^{30}Si). The $bSiO_2$ dissolution rates were assessed from the increase in ^{28}Si in the dissolved phase, which resulted from the dissolution of the initial $bSiO_2$. For each light level, 8 l of seawater were collected in a polycarbonate bottle; 2 l were then filtered immediately to serve as the natural abundance reference for sample bracketing during isotopic analysis back at the home laboratory (see below, this section, and Fripiat et al. 2009). The remaining 6 l were spiked with ^{30}Si and homogenized. A second 2 l aliquot was filtered for the initial conditions after spike addition, and the remaining volume was incubated in a 4 l polycarbonate bottle. After 24 h (t24) of incubation, a 2 l subsample was filtered, and the final 2 l was filtered after 48 h (t48).

It is common experimental practice to limit the ^{30}Si-spike addition to <10% of the initial concentration, so that the system is not excessively perturbed (Nelson & Goering 1977a,b). Nevertheless, 12 of our 36 incubations had a tracer addition of between +10% and +20%, and 1, of more than +30%. However, as shown later, the high degree of consistency between ^{30}Si-uptake results and ^{32}Si-uptake results for which Si additions were always <10% suggests that results have not been biased by over-addition of ^{30}Si (see 'Results—Comparison between t24 and t48 and uptake rates from ^{32}Si and ^{30}Si methods').

$Si(OH)_4$ was analyzed on board using a segmented flow auto-analyzer (Lachat Quickchem Series 8000 FIA), and $bSiO_2$ was filtered (2 l) onto polycarbonate membranes (47 mm diameter Nuclepore filters, 0.4 µm porosity). These were dried at 60°C and stored at room temperature. On return to the laboratory, $bSiO_2$ was digested during a 1-step process (adapted from Ragueneau et al. 2005) using 0.2 M NaOH and heating at 100°C for 40 min. Digests were subsequently neutralized with 1 M HCl. The $bSiO_2$ concentrations were determined colorimetrically using a spectrophotometer (Genesys 10S UV) following the procedure of Grasshoff et al. (1983).

For assessing the ^{30}Si atomic percent of $Si(OH)_4$ (isotopic abundance) we applied a preconcentration protocol adapted from the MAGIC method (adapted according to Karl & Tien 1992). The $Si(OH)_4$ present in 1 l of filtered seawater was scavenged by a brucite ($Mg[OH]_2$) precipitate obtained by increasing pH with a 14 µM NaOH solution (1 ml l^{-1}). The $Mg(OH)_2$ precipitate was dissolved with 3 µM HCl (4.3 ml). This preconcentration step increases the $Si(OH)_4$:salinity ratio of the samples in a step considered beneficial for inductively coupled plasma–mass spectrometry (ICP-MS) analysis, as highly saline solutions may clog the plasma interface (Fripiat et al. 2009). Regardless, mixed layer $Si(OH)_4$ concentrations were still very low during the SAZ-Sense cruise (<2.8 µmol l^{-1}; except for the 1% PAR depth at P2) to allow for direct analysis of the isotopic abundance without prior purification (dilution of the preconcentrated solution is too low; Fripiat et al. 2009). Therefore, we removed the saline matrix from all samples by cation-exchange chromatography (BioRad cation exchange resin DOWEX 50W-X12 [200 to 400 mesh] in H^+ form) using a protocol adapted from Georg et al. (2006). The Si species do not bind to the resin, which effectively retains most seawater cationic species. The method allowed for the complete recovery of Si.

Purified $Si(OH)_4$ samples and digested $bSiO_2$ solutions were diluted to ~100 ppb Si in double-distilled 0.65% HNO_3 and analyzed for ^{30}Si isotopic abundance (in ^{30}Si at.%, = 100% [^{30}Si] / ([^{28}Si] + [^{29}Si] + [^{30}Si])), by

high resolution–sector field–ICP-MS (HR-SF-ICP-MS, ELEMENT2; Thermo) in wet plasma (Fripiat et al. 2009). The instrumental mass bias was corrected by the standard bracketing methodology. As described above, the standard consists of an unspiked sample treated in the same way as the spiked samples, thus avoiding any matrix effect. Each analysis was duplicated, and the reproducibility of ^{30}Si isotopic abundance (at.%) was better than 1% (relative standard deviation). This method is much easier and faster than methods using an isotope ratio mass spectrometer (Nelson & Goering 1977a) or a quadrupole thermal ionization mass spectrometer (Corvaisier et al. 2005).

The production (= Si-uptake at such incubation time scale) and dissolution rates of $bSiO_2$ (respectively, ρ_{uptake} and ρ_{diss}) were calculated using a model. We tested the linear 1-compartmental model developed for assessing production (Nelson & Goering 1977a) and dissolution (Nelson & Goering 1977b) and the non-linear 2-compartmental model developed by Elskens et al. (2007). The classical approach for assessing $bSiO_2$ production and dissolution following the linear 1-compartmental model is derived as follows:

$$\xrightarrow{(\rho,æ)}(C,æ_C) \quad (1)$$

where C represents either $bSiO_2$ or $Si(OH)_4$ concentrations, $æ_C$ is the ^{30}Si isotopic abundance in excess (by subtracting the natural ^{30}Si isotopic abundance) either of $bSiO_2$ or $Si(OH)_4$ and ρ is either the $bSiO_2$ production or dissolution fluxes. By integration of the differential equation associated with this model, the $bSiO_2$ production and dissolution can be solved as follows:

$$\rho_{prod} = \frac{æ_{bSiO_2\ (t_f)}}{æ_{Si(OH)_4\ (t_0)} \cdot t} \cdot [bSiO_2] \quad (2)$$

$$\rho_{diss} = \frac{æ_{Si(OH)_4\ (t_0)} - æ_{Si(OH)_4\ (t_f)}}{æ_{Si(OH)_4\ (t_0)} \cdot t} \cdot [Si(OH)_4] \quad (3)$$

with t_0 and t_f representing the initial and final incubation times. The mass and isotopic balance operating during the course of the incubation is not taken into account in the 1-compartmental model. In the 2-compartmental model, parameters are constrained by the requirement to fit mass and isotopic balances of dissolved and particulate phases (Elskens et al. 2007). It is derived as follows:

$$([Si(OH)_4], æ_{Si(OH)_4}) \xleftarrow{(\rho_{prod}, æ_{Si(OH)_4})-(\rho_{diss}, æ_{bSiO_2})} ([bSiO_2], æ_{bSiO_2}) \quad (4)$$

The important features of the 2-compartmental model are that (1) all Si atoms that leave the dissolved phase appear as $bSiO_2$ and (2) all Si atoms that leave $bSiO_2$ appear as $Si(OH)_4$. The latter model takes into account any isotopic dilution and concentration changes occurring over the course of the incubation, which, when ignored, may induce significant bias (Elskens et al. 2007). The 2 models have been tested on the SAZ-Sense data and are compared in the section 'Results — Choice of model'.

Si-uptake estimates from ^{30}Si and ^{32}Si methods were compared for most of the incubation experiments (32 out of 36). For the ^{32}Si method, 275 ml seawater samples were spiked with 800 Bq of radioactive ^{32}Si isotope ($^{32}Si[OH]_4$, specific activity 19.97 KBq μg^{-1} Si; corresponding to an addition of Si of 0.006 $\mu mol\ l^{-1}$ $sample^{-1}$) produced by the Los Alamos laboratory (Tréguer et al. 1991) and incubated for 24 h in the same deck incubators used for ^{30}Si. After 24 h, the samples were filtered (0.4 µm porosity, polycarbonate membranes) and filters were stored in PE scintillation vials at ambient temperature until analysis. ^{32}Si-uptake rates were assessed by measuring the retained radioactivity in Cerenkov counting (Bq, number of disintegrations per second) on the filters using a Packard 1600-TR scintillation counter (Tréguer et al. 1991) and the following model described in Brzezinski et al. (1997):

$$\rho_{prod} = \frac{Bq_{bSiO_2}}{Bq_{\ Total} \cdot t} \cdot [Si(OH)_4] \quad (5)$$

Since dissolving $bSiO_2$ has a negligible ^{32}Si radioactivity, the dissolution of $bSiO_2$ in the ^{32}Si-enriched $Si(OH)_4$ pool (high specific activity) does not affect its radioactivity (number of disintegration per second). For this reason, there are no significant biases induced by the choice of a model for production fluxes calculated using the ^{32}Si method, in contrast to those calculated by ^{30}Si with the 1-compartmental model described above. The relative precision of ^{32}Si-uptake rates is 10%, similar to the ^{30}Si method.

The specific Si-uptake rate (V_{Si}; d^{-1}) gives the fraction of the $bSiO_2$ pool produced in 1 d as follows:

$$V_{Si} = \frac{\rho_{prod}}{[bSiO_2]} \quad (6)$$

From Eq. (4) we can calculate the doubling time (Td; d^{-1}) assuming exponential growth:

$$Td = \frac{\ln(2)}{V_{Si}} \quad (7)$$

RESULTS

Accuracy of the $bSiO_2$ production and dissolution rates

Detection limit of the $bSiO_2$ dissolution rate

No significant variations in the ^{30}Si $Si(OH)_4$ atomic percent were observed over the various durations encompassed by the different incubation experiments conducted in the eastern SAZ, or for the last incuba-

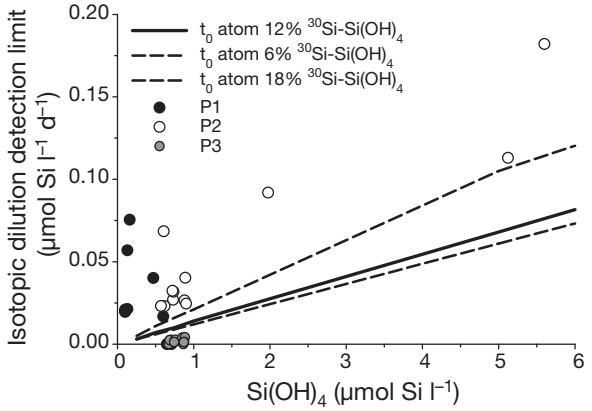

Fig. 2. Detection limit of ^{28}Si-isotopic dilution for measuring biogenic silica ($bSiO_2$) dissolution as a function of $Si(OH)_4$ concentration and ^{30}Si spike addition. Circles represent the SAZ-Sense dataset. The continuous line represents the detection limit for a 10% spike addition; the dashed lines show ±5%. P1, P2, and P3: Process locations; t_0: initial incubation time

tion experiment in the western SAZ. The results indicate $bSiO_2$ dissolution in these experiments was too small to be detected. Larger ^{30}Si-spike additions, as in Brzezinski et al. (2001), would have increased the sensitivity of the method. Unfortunately, such experiments were not performed on board during the SAZ-Sense study. To improve the sampling strategy in the future, the detection limit for ^{28}Si-isotopic dilution was estimated by solving the mass and isotopic balance for incubations where the difference between initial and final ^{30}Si-isotopic abundances were set at 1% (~1 relative standard deviation analytical precision; Fripiat et al. 2009) (Fig. 2). The $bSiO_2$ production and concentration had no significant influence on the detection limit of $bSiO_2$ dissolution. We tested the effect of the $Si(OH)_4$ concentration (from 0.25 to 6 µmol l^{-1}) and initial $Si(OH)_4$ ^{30}Si-isotopic abundances (12 ± 6 at.% ^{30}Si, i.e. a spike addition of ~10 ± 5%). The detection limit of the $bSiO_2$ dissolution rate as a function of $Si(OH)_4$ concentration follows a linear relationship. The detection limit of the $bSiO_2$ dissolution rate (µmol Si l^{-1}) for a 10% spike addition was determined at 0.014 × [$Si(OH)_4$] (µmol l^{-1}). The detection limit for the eastern SAZ (P3) experiments and the final experiment in the western SAZ (P1) was estimated at ~0.010 µmol Si l^{-1} d^{-1}.

Choice of model

In order to assess the discrepancy between the observations (y_i) and the model counterparts (x_i) for the 4 parameters used ([$Si(OH)_4$], [$bSiO_2$], $^{30}Si_{bSiO_2}$ isotopic abundance and $^{30}Si_{Si(OH)_4}$ isotopic abundance), the residual ($y_i - x_i$) needs to be transformed to a common scale by the standardized residual (SR_i) approach (Elskens et al. 2007):

$$SR_i = \frac{y_i - x_i}{\sqrt{2}\cdot\sigma_i} \quad (8)$$

where σ_i represents the relative standard deviation expected for each parameter. Thus, SR_i represents the deviation of the modeled value from the measurement value normalized by the expected uncertainty of the parameter. Considering the complete set of sampling treatments and analyses, we consider relative standard deviations of 2, 7 and 1% for [$Si(OH)_4$], [$bSiO_2$], and ^{30}Si-isotopic abundances, respectively. Compared to the initial methodology published in Fripiat et al. (2009), estimates of the standard deviations were further refined using data acquired for 42 triplicate ^{30}Si incubations during the BONUS-GoodHope cruise (RV 'Marion Dufresne' in 2008) (Fripiat 2010). In cases where the model successfully describes the main features of the uptake and dissolution processes, it was expected that SR_i scores for each parameter would be symmetrically distributed around a mean of zero and <3, i.e. <3 times the expected standard deviation (Elskens et al. 2007).

The 2 models (see 'Materials and methods—Production and dissolution rates of $bSiO_2$') fit the ideal zero-centered distribution (Fig. 3), even though the 2-compartmental model appears to more adequately describe the mass and isotopic balance than the 1-compartmental model. Only SR_i scores for incubations where $bSiO_2$ dissolution rates were above the detection limit are shown in Fig. 3 (see 'Results—Detection limit of the $bSiO_2$ dissolution rate'). At t48 the models do not perfectly fit the zero-centered distribution, but generally the outcomes still fit within the expected experimental uncertainties, except for $æ_{Si(OH)_4}$ in the 1-compartmental model (Fig. 3b). Generally, the 1-compartmental model yielded acceptable results, but the SR_i scores were always better under the 2-compartmental model. Therefore, the uptake and dissolution rates calculated with the 2-compartmental model will be discussed. Note that actual measurements of $bSiO_2$ and $Si(OH)_4$ concentrations (and not optimized contents recalculated from the models) are used in both the model and discussion.

Comparison between t24 and t48 and uptake rates from ^{32}Si and ^{30}Si methods

Si-uptake rates estimated at t24 and t48 were not significantly different (Table 1; slope = 1.01 ± 0.03, R^2 = 0.94, n = 36, $p < 0.01$). Si-uptake estimated via ^{30}Si and ^{32}Si methods were also compared for the complete set of incubations (Table 1). A good correlation for the

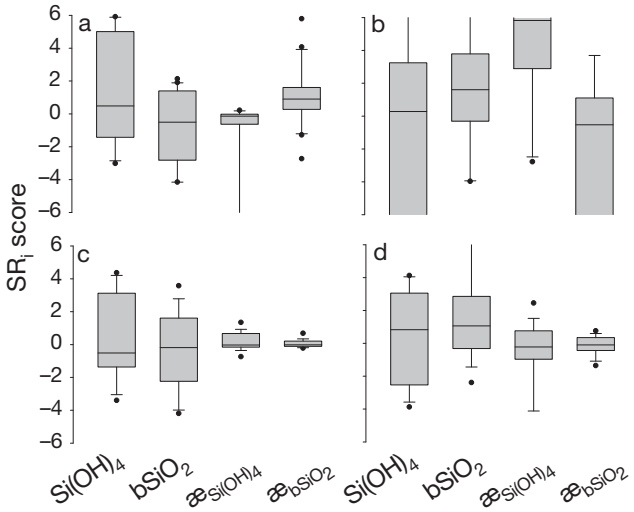

Fig. 3. SR_i scores for the 1-compartmental model for (a) t24 and (b) t48 and for the 2-compartmental model for (c) t24 and (d) t48. Only values where $bSiO_2$ dissolution is above the detection limit are shown (see 'Results—Detection limit of the $bSiO_2$ dissolution rate'). $Si(OH)_4$, $bSiO_2$, $æ_{Si(OH)4}$ and $æ_{bSiO2}$ are silicic acid and biogenic silica concentrations, and ^{30}Si isotopic abundance in excess for silicic acid and biogenic silica, respectively. The boxes, whiskers and symbols cover the 25th to 75th, the 10th to 90th and the 5th to 95th percentiles, respectively

whole data set between the 2 methods was obtained (slope = 0.96 ± 0.06, R^2 = 0.85, n = 32, $p < 0.01$). At P3, however, ^{32}Si-uptake rates exceeded ^{30}Si-uptake rates, yet the former uptake rates were still very low (<12 nmol Si d^{-1}; Table 1). At this station, $bSiO_2$ concentrations of ^{30}Si-spiked incubations were systematically higher than for ^{32}Si samples (0.025 ± 0.004 [1 SD] and 0.016 ± 0.001 [1 SD] µmol l^{-1}, respectively, Mann-Whitney rank sum test, $p < 0.001$), suggesting possible Si-contamination. Any contamination with Si having natural isotopic composition would have decreased the final ^{30}Si-isotopic abundance of $bSiO_2$, thereby leading to an underestimation of the true Si-uptake.

The $bSiO_2$ dissolution rates from t24 and t48 were also very similar (Table 1; slope = 0.91 ± 0.05, R^2 = 0.86, n = 35, $p < 0.01$, 1 outlier excluded). The outlier represents the deep $bSiO_2$ maximum at P2 in the PFZ (Cast 58, 1% PAR), where $bSiO_2$ dissolution at t24 largely exceeded dissolution at t48. For the deep $bSiO_2$ maximum at P2, the t48 ^{30}Si-uptake was closer to t24 ^{32}Si-uptake and achieved a better SR_i score than the ^{30}Si-uptake at t24 (not shown).

To summarize, the following results will be used in the discussion (Table 1): (1) Si-uptake rates are based

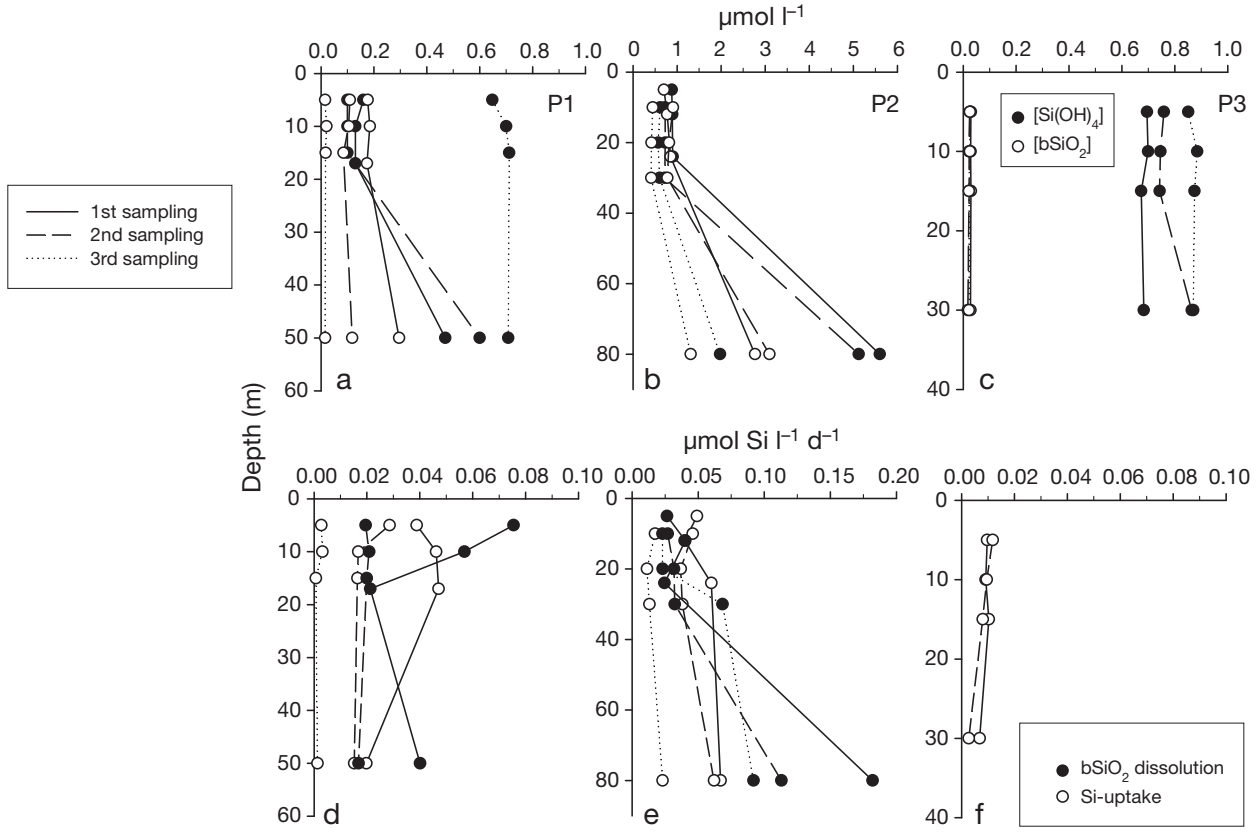

Fig. 4. (a,b,c) Vertical distribution of $Si(OH)_4$ and $bSiO_2$ (µmol l^{-1}) and (d,e,f) $bSiO_2$ production and dissolution (µmol Si l^{-1} d^{-1}) in the euphotic layer (100–50 to 25–1% photosynthetically active radiation). Process 1 (P1, western SAZ) is shown in Panels a and d, Process 2 (P2, PFZ) is shown in Panels b and e, and Process 3 (P3, eastern SAZ) is shown in Panels c and f. PFZ: Polar Frontal Zone; SAZ: Subantarctic Zone

Table 1. $[Si(OH)_4]$, $[bSiO_2]$, Si-uptake (ρ_{uptake}, both with ^{30}Si and ^{32}Si), $bSiO_2$ dissolution (ρ_{diss}) for each cast of each process station. The italic values for $bSiO_2$ dissolution are below the detection limit (see section 'Detection limit of the $bSiO_2$ dissolution rate'). PAR: photosynthetically active radiation; na: not available. Bold values for $bSiO_2$ concentration, ρ_{uptake}, and ρ_{diss} are the ones used in the 'Discussion' (section 'Comparison between t24 and t48 and uptake rates from ^{32}Si and ^{30}Si methods')

Station sampling date 2007	Cast no.	PAR (%)	Depth (m)	Temp. (°C)	$Si(OH)_4$ (µmol l^{-1})	$bSiO_2$ (µmol l^{-1})		ρ_{uptake} (^{30}Si) (µmol l^{-1} d^{-1})		ρ_{uptake} (^{32}Si) (µmol l^{-1} d^{-1})	ρ_{diss} (^{30}Si) (µmol l^{-1} d^{-1})		V_{Si} (d^{-1})	V_{diss} (d^{-1})
						^{30}Si	^{32}Si	t24	t48	t24	t24	t48		
Process 1														
22 Jan	9	100	5	13.1	0.16	**0.176**	0.200	**0.039**	na	0.044	**0.075**	0.088	0.22	0.43
		50	10	13.0	0.13	**0.184**	0.210	**0.046**	na	0.033	**0.057**	0.091	0.25	0.31
		25	17	12.9	0.13	**0.174**	0.205	**0.047**	0.031	0.019	**0.021**	0.041	0.27	0.12
		1	50	12.1	0.47	**0.295**	0.295	**0.020**	0.021	0.036	**0.040**	0.036	0.07	0.14
24 Jan	17	100	5	12.8	0.10	**0.109**	0.126	**0.029**	0.029	0.033	**0.020**	0.020	0.26	0.18
		50	10	12.8	0.10	**0.105**	0.131	**0.017**	0.015	0.021	**0.021**	0.012	0.16	0.20
		25	15	12.8	0.10	**0.085**	0.076	**0.016**	0.018	0.026	**0.020**	0.011	0.19	0.23
		1	50	11.3	0.60	**0.118**	0.168	**0.015**	na	0.015	**0.017**	na	0.13	0.14
29 Jan	34	100	5	11.3	0.65	**0.016**	0.026	**0.003**	0.003	0.001	*0.000*	*0.000*	0.18	na
		50	10	11.3	0.70	**0.020**	0.025	**0.003**	0.004	0.001	*0.002*	*0.000*	0.16	na
		25	15	11.3	0.71	**0.017**	0.025	**0.001**	0.000	0.001	*0.001*	*0.000*	0.04	na
		1	50	11.3	0.71	**0.016**	0.025	**0.001**	0.001	0.003	*0.000*	*0.000*	0.08	na
Process 2														
2 Feb	42	100	5	5.4	0.88	**0.702**	0.774	**0.049**	0.057	0.065	**0.027**	0.022	0.07	0.04
		50	12	5.4	0.89	**0.777**	0.858	**0.040**	0.046	0.057	**0.040**	0.011	0.05	0.05
		25	24	5.4	0.90	**0.852**	0.980	**0.060**	0.068	0.044	**0.025**	0.020	0.07	0.03
		1	80	2.2	5.60	**2.768**	2.703	0.074	**0.067**	0.064	0.217	**0.182**	0.02	0.07
3 Feb	47	100	10	5.3	0.73	**0.909**	0.508	**0.046**	0.050	0.044	**0.027**	0.026	0.05	0.03
		50	20	5.3	0.73	**0.817**	0.392	**0.037**	0.043	0.050	**0.032**	0.024	0.05	0.04
		25	30	5.3	0.72	**0.782**	0.392	**0.038**	0.039	0.027	**0.032**	0.043	0.05	0.04
		1	80	2.2	5.12	**3.098**	3.036	na	**0.062**	0.046	0.087	**0.113**	0.02	0.04
6 Feb	58	100	10	5.2	0.62	**0.450**	0.277	**0.017**	0.015	0.016	na	**0.023**	0.04	0.05
		50	20	5.2	0.57	**0.418**	0.277	**0.011**	0.009	0.014	**0.023**	0.009	0.03	0.06
		25	30	5.2	0.61	**0.412**	0.323	**0.013**	0.010	0.013	na	**0.068**	0.03	0.17
		1	80	3.5	1.98	**1.310**	1.549	0.014	**0.023**	0.027	0.364	**0.092**	0.02	0.07
Process 3														
12 Feb	81	100	5	13.6	0.70	0.029	**0.016**	0.001	0.005	**0.010**	*0.001*	*0.004*	0.60	na
		50	10	13.6	0.70	0.028	**0.016**	0.001	0.003	**0.009**	*0.001*	*0.005*	0.56	na
		25	15	13.3	0.67	0.029	**0.016**	0.004	0.001	**0.010**	*0.000*	*0.008*	0.64	na
		1	30	12.6	0.68	0.028	**0.016**	0.002	0.002	**0.007**	*0.002*	*0.004*	0.42	na
13 Feb	85	100	5	13.3	0.76	0.025	**0.014**	0.003	0.004	**0.012**	*0.003*	*0.003*	0.87	na
		50	10	13.4	0.75	0.022	**0.016**	0.003	0.006	**0.010**	*0.001*	*0.000*	0.59	na
		25	15	13.6	0.74	0.022	**0.016**	0.003	0.007	**0.008**	*0.001*	*0.001*	0.49	na
		1	30	12.3	0.86	0.018	**0.015**	0.001	0.001	**0.003**	*0.000*	*0.001*	0.18	na
15 Feb	96	100	5	13.6	0.85	0.025	na	0.003	0.006	na	*0.004*	*0.003*	na	na
		50	10	13.6	0.89	0.025	na	0.004	0.005	na	*0.004*	*0.000*	na	na
		25	15	13.6	0.88	0.022	na	0.001	0.002	na	*0.001*	*0.000*	na	na
		1	30	13.0	0.87	0.022	na	0.001	0.002	na	*0.001*	*0.002*	na	na

on results from t24 incubation experiments, except (a) for the deep (1% PAR) P2 samples for which results from t48 incubations were used and (b) for P3 samples with uptake results deduced from ^{32}Si experiments; and (2) $bSiO_2$ dissolution rates were based on results from the t24 incubation experiments, with the exception of the deep P2 samples (1% PAR) where dissolution results were based on results from the t48 incubations.

Production and dissolution of $bSiO_2$ across the SAZ-Sense data

The mixed layer in the western SAZ (P1) had lower and more variable $Si(OH)_4$ concentrations (0.38 ± 0.28 µmol l^{-1}) than in the eastern SAZ (P3; 0.78 ± 0.08 µmol l^{-1}) and the PFZ (P2; 0.74 ± 0.13 µmol l^{-1}), both stations having indistinguishable $Si(OH)_4$ concentrations (Fig. 4a,b,c). Kruskal-Wallis 1-way analysis

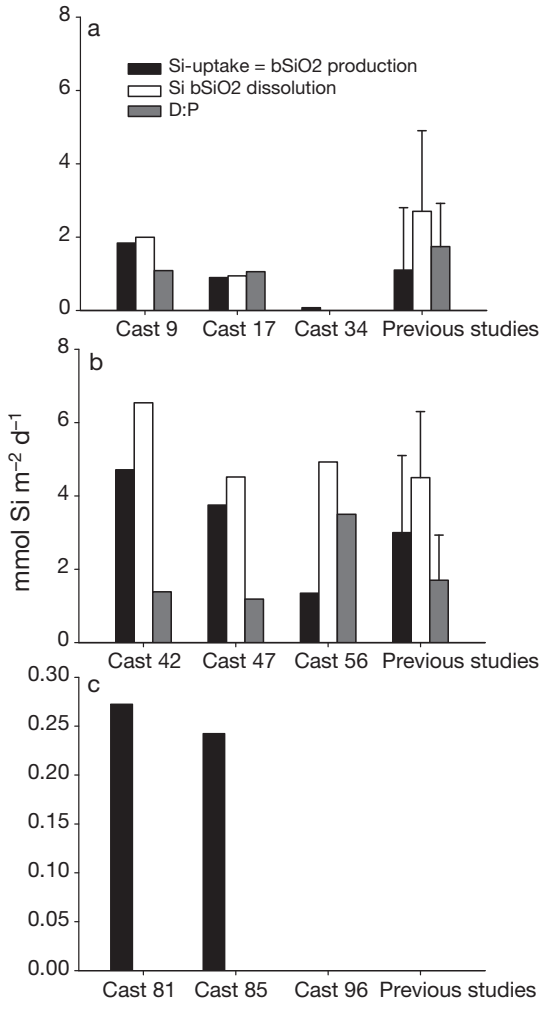

Fig. 5. Integrated (100 to 1% photosynthetically active radiation) $Si(OH)_4$ uptake (i.e. $bSiO_2$ production) and $bSiO_2$ dissolution rates, and dissolution:production ratios (D:P). Panels a, b, and c represent P1 (western SAZ), P2 (PFZ), and P3 (eastern SAZ), respectively. Previous studies show the summer values of earlier studies for each area (Caubert 1998, Brzezinski et al. 2001, Quéguiner 2001, Leblanc et al. 2002, Beucher et al. 2004). PFZ: Polar Frontal Zone; SAZ: Subantarctic Zone. Values for Cast 96 were below detection limit, and no previous studies are available for the eastern SAZ (Panel C)

indicated that the 3 stations are significantly different ($p < 0.001$). Dunn's post hoc comparison indicated that, indeed, the western SAZ $Si(OH)_4$ concentration was significantly lower ($p < 0.05$) than those of the the eastern SAZ and PFZ, which were similar ($p > 0.05$). The $Si(OH)_4$ concentration in the SAZ subsurface layers was rather uniform, though showing a slight increase with depth ([$Si(OH)_4$] at 400 m ≈ 5 µmol l^{-1}; Fig. 4a,b). In contrast, a large vertical gradient was observed in the PFZ ([$Si(OH)_4$] at 400 m ≈ 70 µmol l^{-1}; Fig. 4c).

The mixed layer $bSiO_2$ concentrations were highest in the PFZ (0.68 ± 0.20 µmol l^{-1}), intermediate in the western SAZ (0.11 ± 0.09 µmol l^{-1}), and lowest in the eastern SAZ (0.02 ± 0.00 µmol l^{-1}; Fig. 4a,b,c). Kruskal-Wallis 1-way analysis confirmed that there is a difference among the stations ($p < 0.001$). Nevertheless, Dunn's post hoc comparison indicated that the value in the PFZ was significantly higher ($p < 0.05$) than those in the eastern and western SAZ, which were similar ($p > 0.05$). In the PFZ, below the mixed layer, a $bSiO_2$ maximum (2.39 ± 0.95 µmol l^{-1}) was associated with a subsurface chl *a* maximum. This is a recurrent feature in this area (Parslow et al. 2001, Quéguiner 2001).

As observed from the $bSiO_2$ concentration results, the mixed layer Si-uptake (ρ_{Si}) was highest in the PFZ (0.035 ± 0.017 µmol l^{-1} d^{-1}), intermediate in the western SAZ (0.020 ± 0.017 µmol l^{-1} d^{-1}), and lowest in the eastern SAZ (0.008 ± 0.003 µmol l^{-1} d^{-1}; Fig. 4d,e,f). Kruskal-Wallis 1-way analysis indicated that there is a significant difference among the 3 stations ($p = 0.001$). According to Dunn's post hoc comparison, the significant difference is between the PFZ and eastern SAZ ($p < 0.05$). In the PFZ, a slight increase in the Si-uptake rate coincided with the $bSiO_2$ maximum (0.051 ± 0.024 µmol l^{-1} d^{-1}), although this increase was not significant when contrasted with the large increase in the $bSiO_2$ concentration. Our integrated Si-uptake rates are indistinguishable from results previously published for the SAZ and PFZ (Fig. 5; Caubert 1998, Brzezinski et al. 2001, Quéguiner 2001, Leblanc et al. 2002, Beucher et al. 2004). We are unaware of any study reporting Si-uptake rates for other naturally iron-fertilized SAZ areas similar to those encountered at P3 (see Bowie et al. 2009, Lannuzel et al. 2011).

During the SAZ-Sense study, specific Si-uptake rates (V_{Si}; d^{-1}) varied widely between the studied sites (Fig. 6a; Eq. 6). The occurrence of such a gradient of specific Si-uptake rates has also been observed by others along 2 transects, with rates increasing from 0.01 to 0.40 d^{-1} between the PFZ and STZ (Quéguiner 2001, Leblanc et al. 2002). Specific uptake rates at the different SAZ-Sense sites, on the contrary, remained quite uniform over time—PFZ: 0.02 to 0.07 d^{-1} with a doubling time from 10 to 40 d; western SAZ: 0.04 to 0.27 d^{-1} with a doubling time from 3 to 17 d; and eastern SAZ: 0.18 to 0.87 d^{-1} with a doubling time from 1 to 4 d. The values in the eastern SAZ were especially high for the Southern Ocean, compared to published results of specific uptake rates, which do not exceed 0.32 d^{-1} (Nelson & Gordon 1982, Brzezinski et al. 2001, Quéguiner 2001, Leblanc et al. 2002, Beucher et al. 2004).

Across the SAZ-Sense area, $bSiO_2$ dissolution (i.e. ρ_{diss}) generally exceeded, or was slightly lower, than production (Fig. 4d,e,f). The mixed layer $bSiO_2$ dissolution rates were similar (Mann-Whitney rank sum test, $p = 0.27$) between the PFZ (0.033 ± 0.014 µmol Si l^{-1} d^{-1})

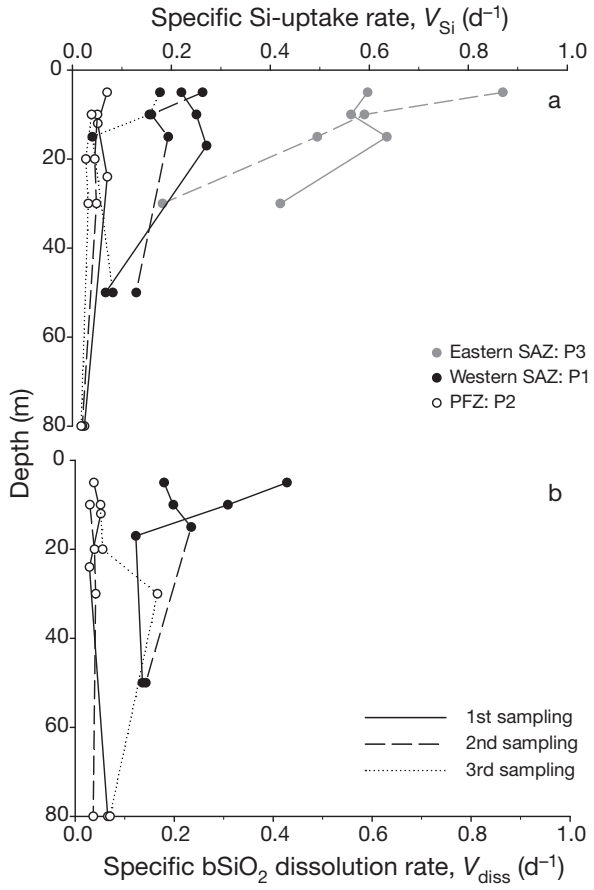

Fig. 6. Vertical distribution of specific (a) Si-uptake and (b) $bSiO_2$ dissolution rates for each cast of each process station, except for stations below the detection limit for $bSiO_2$ dissolution rates (P3 and third sampling of P1). The black, white, and gray dots represent Process Stations 1, 2, and 3 (P1 to P3), respectively. For P3, only the ^{32}Si results are presented (see 'Materials and methods'). PFZ: Polar Frontal Zone; SAZ: Subantarctic Zone

and the western SAZ (first 2 experiments only: 0.034 ± 0.022 µmol Si l^{-1} d^{-1}), except for the deep $bSiO_2$ maximum in the PFZ where the highest rates were measured (0.129 ± 0.047 µmol Si l^{-1} d^{-1}). Dissolution rates were below the detection limit in the eastern SAZ and, for the last experiments, in the western SAZ (both <0.010 µmol Si l^{-1}) (see 'Results—Detection limit of the $bSiO_2$ dissolution rate'). Integrated $bSiO_2$ dissolution in the western SAZ and in the PFZ were in the range reported by others for the summer period (Fig. 5; Brzezinski et al. 2001, Beucher et al. 2004).

Higher specific $bSiO_2$ dissolution rates ($V_{diss} = \rho_{diss}/[bSiO_2]$; d^{-1}) were observed in the western SAZ than in the PFZ (Mann-Whitney rank sum test, $p < 0.001$; 0.22 ± 0.10 and 0.06 ± 0.04 d^{-1}, respectively; Fig. 6b). Published values of V_{diss} in the PFZ and SAZ range from 0.01 to 0.13 d^{-1} (Nelson & Gordon 1982, Brzezinski et al. 2001, Beucher et al. 2004).

DISCUSSION

Control of $bSiO_2$ production and dissolution rates

Production rates

The contribution of any detrital $bSiO_2$ would underestimate the specific uptake rate (V_{Si}; d^{-1}) since the latter is obtained by normalizing the uptake rate to the bulk $bSiO_2$ concentration (living + detrital; Eq. 4). The contribution of detrital $bSiO_2$ to bulk $bSiO_2$ was not measured during the SAZ-Sense study. Using the PDMPO probe, Leblanc & Hutchins (2005) observed that, in general, only certain diatom species in the bulk diatom community were actively taking up Si, though the situation was different in the eastern SAZ (see below). Since only a small fraction of $bSiO_2$ was actively silicifying, it follows that bulk specific uptake rates were probably significantly underestimated. Taking the largest value for the relative contribution of dead diatom cells to bulk diatom abundance, reported for the Southern Ocean (i.e. 0.5; Beucher et al. 2004, Armand et al. 2008), our V_{Si} values increased from 0.04 to 0.07 d^{-1} and from 0.22 to 0.36 d^{-1} for the PFZ and western SAZ, respectively. It thus appears that the contribution of any non-living diatom-associated $bSiO_2$ is unlikely the main reason for the observed V_{Si} distribution (Fig. 6a).

A relatively large number of studies have examined the kinetics of Si-uptake by both natural diatom assemblages and cultured clones. V_{Si} (d^{-1}) generally increases with increasing extracellular $Si(OH)_4$ in a way that closely follows the Michaelis-Menten saturation function (e.g. Del Amo & Brzezinski 1999, Thamatrakoln & Hildebrand 2008):

$$V_{Si} = \frac{[Si(OH)_4] \cdot V_{max}}{[Si(OH)_4] + K_{Si}} \quad (9)$$

where V_{max} (d^{-1}) represents the maximum rates of uptake at infinite substrate concentration and K_{Si} (µmol l^{-1}) is the $Si(OH)_4$ concentration at $0.5 V_{max}$. K_{Si} is inversely proportional to the diatom (Si-) affinity, e.g. the relative ability of diatoms to use low levels of $Si(OH)_4$. During the SAZ-Sense study a strong gradient in V_{Si} (from 0.02 to 0.87 d^{-1}) was observed despite similar $Si(OH)_4$ concentrations (~0.7 µmol l^{-1}), exceptions were noted at the 2 first stations in the western SAZ and for the deep PFZ $bSiO_2$ maximum (Fig. 7). However, these outliers were also different compared to the trend expected from Eq. (9), as they either revealed an intermediate V_{Si} with a lower $Si(OH)_4$ concentration or a lower V_{Si} regardless of higher $Si(OH)_4$ concentrations. This uncoupling of V_{Si} (d^{-1}) from the $Si(OH)_4$ concentration, suggests differences in kinetic parameters (V_{max} and K_{Si}) related to differences in biogeochemical

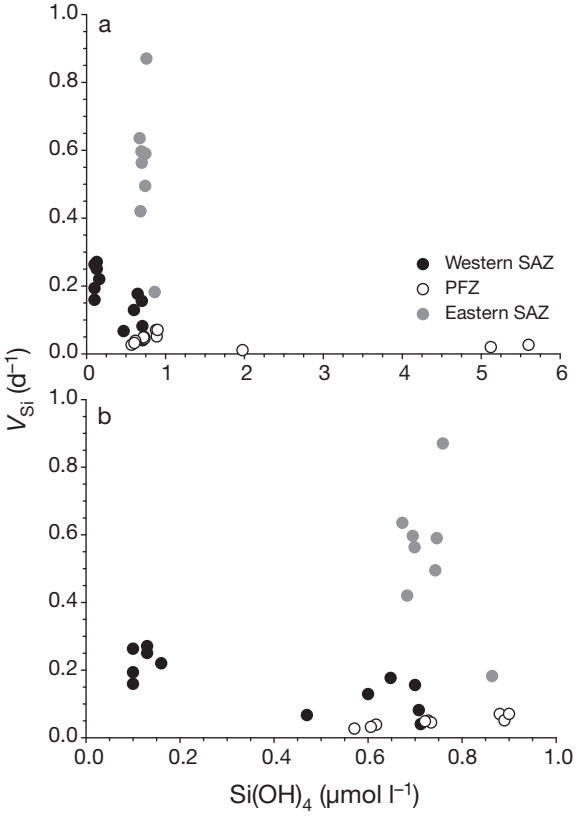

Fig. 7. Specific Si-uptake versus $Si(OH)_4$ concentration for the 3 process stations—black: western SAZ (P1); white: PFZ (P2); gray: eastern SAZ (P3). Panel b shows $Si(OH)_4$ on a smaller scale (<1 µmol l^{-1}). Consequently, the deep PFZ $bSiO_2$ maximum is not seen in Panel b. PFZ: Polar Frontal Zone; SAZ: Subantarctic Zone

conditions and/or diatom communities (Cassar et al. 2011, de Salas et al. 2011).

During summer different co-limitations are expected for the PFZ and SAZ, and these could influence the Si-uptake mechanism, thus providing an explanation for the observed V_{Si} distribution (Boyd et al. 1999, De La Rocha et al. 2000, Franck et al. 2000, 2003, Hutchins et al. 2001, Leynaert et al. 2004). $Si(OH)_4$, nitrate and phosphate concentrations increased with latitude and with depth from the STZ to the PFZ in the present study. Nitrate and phosphate were expected to be non-limiting (Sedwick et al. 2002, Bowie et al. 2009). Although the $Si(OH)_4$ concentration (<1 µmol l^{-1}) was near or below the half-saturation constants for Si-uptake (from 0.7 to 10 µmol l^{-1}; Nelson et al. 2001), V_{Si} (d^{-1}) was independent of the $Si(OH)_4$ concentration (Fig. 7). The dissolved iron concentration generally decreased from north to south (Bowie et al. 2009, Lannuzel et al. 2011). This gradient is most likely due to a large supply of iron further north, from both the advection of East Australian Current iron-rich subtropical waters and the Aeolian deposition of dust coming from the Australian continent (Bowie et al. 2009). Cassar et al. (2011) provide evidence for the critical roles of iron and light as limiting factors for primary production across the SAZ-Sense area: the net community production was: (1) strongly correlated with dissolved iron concentration and iron sufficiency and (2) uncorrelated with mixed layer depth. Such co-limitations are likely to have impacted Si-uptake processes and consequently Si-uptake kinetic parameters (Eq. 9; De La Rocha et al. 2000, Claquin et al. 2002, Franck et al. 2000, 2003, Leynaert et al. 2004). During the SAZ-Sense cruise iron limitation matched with V_{Si} distribution, both showing higher values in the eastern SAZ, intermediate values in the western SAZ, and lowest values in the PFZ (Fig. 6a). Also V_{Si} shows a decreasing trend with depth along with light availability (Fig. 6a). Although the cellular silicon cycle (the $bSiO_2$ polymerization process) is not strictly light dependent, photosynthesis is clearly involved in supplying energy, at least for the synthesis of the organic compounds involved in the Si-uptake machinery (Martin-Jézéquel et al. 2000, Claquin et al. 2002). Our data suggest that, despite the decoupling of cell Si and C cycles, Si-uptake kinetics are not strictly independent of light levels.

Diatom communities differed between the SAZ and PFZ, with lightly silicified pennate diatoms in the former and heavily silicified diatoms (pennate and centric diatoms) in the latter (de Salas et al. 2011). It is likely that SAZ diatom communities are adapted to year-round low $Si(OH)_4$ concentrations (<4 to 5 µmol l^{-1}). In the PFZ, relatively high $Si(OH)_4$ concentrations at the onset of the growth period (>10 µmol l^{-1}; Rintoul & Bullister 1999, Cardinal et al. 2005) combined with a strong iron/light co-limitation could favor the growth of heavily silicified diatoms that could efficiently deplete the $Si(OH)_4$ pool (Takeda 1998, Claquin et al. 2002, Franck et al. 2003). It is possible that the late summer PFZ diatom community was poorly adapted to the low $Si(OH)_4$ concentrations, explaining the lower V_{Si} (d^{-1}) values there. Furthermore, large inter- and intra-specific variations of V_{Si} can be expected (De La Rocha et al. 2000, Leynaert et al. 2004, Sarthou et al. 2005). Taken together with the discussed effects of co-limitation this indicates a greater ability of SAZ diatoms to use silicic acid more efficiently at prevailing low $Si(OH)_4$ concentrations, compared to PFZ diatoms.

Dissolution rates

In the marine environment, $bSiO_2$ dissolution has been shown to be influenced by temperature, diatom species composition, trace metal content of the frus-

tules, grazing, bacterial activity, and the relative abundance of dead diatoms (e.g. Ragueneau et al. 2000, Beucher et al. 2004).

During the SAZ-Sense study we observed a positive relationship between $bSiO_2$ concentration and $bSiO_2$ dissolution rates (Table 1; $R^2 = 0.72$, $p < 0.01$, $n = 20$, not shown), suggesting that the contribution of dead diatoms increases with the increase of $bSiO_2$. Higher dissolution rates in the western SAZ and PFZ co-occurred with observations that a large fraction of the diatom community was not silicifying (Leblanc & Hutchins 2005), suggesting that a large fraction of the $bSiO_2$ pool there was detrital. Similarly, Beucher et al. (2004) report a correlation between the fraction of dead diatom cells and $bSiO_2$ dissolution during summer.

The SAZ environment appeared more susceptible to $bSiO_2$ dissolution than that of the PFZ (Fig. 6b). Evidence from the literature indicates that higher temperatures enhance specific $bSiO_2$ dissolution rates (Kamatani 1982, Hurd & Birdwhistell 1983). Therefore, differences in sea surface temperature between these 2 areas (~11 vs. ~5°C, respectively) could, at least in part, explain the difference in specific $bSiO_2$ dissolution rates. Assuming a V_{diss} of 0.06 ± 0.04 d^{-1} (mean PFZ) and the Kamatani (1982) relationship (V_{diss} increases by a factor of 2.27 for each rise in 10°C temperature), V_{diss} should increase from 0.06 ± 0.04 to 0.11 ± 0.05 d^{-1}. It thus appears that higher SAZ temperatures might only partly explain the observed gradient in V_{diss}; though there are uncertainties concerning such a temperature-dependent relationship (Kamatani 1982).

Any process that induces an increase in $bSiO_2$-specific surface and/or a build-up of small amorphous $bSiO_2$ objects with long residence times in surface waters favors $bSiO_2$ dissolution. Based on culture experiments, Schultes et al. (2010) reported enhanced dissolution of $bSiO_2$ following ingestion of diatoms by microzooplankton grazers. Pearce et al. (2011) observed during the SAZ-Sense study that a large fraction of primary production was consumed by microzooplankton and heterotrophic nanoflagellates. Thus, microzooplankton feeding on diatoms could produce light-weight detritus, easily accessible to the hydrolyzing activity of bacteria, which removes the organic matrix from diatom frustules and exposes them to the ambient under-saturated seawater environment (Bidle & Azam 1999). Dumont et al. (2011) report that bacterial activity during the SAZ-Sense study was higher in the SAZ than in the PFZ. To conclude, the conditions favoring a more efficient $bSiO_2$ dissolution in the SAZ (higher V_{diss}) were probably induced by biological processes such as microzooplankton herbivory and bacterial activity (Bidle & Azam 1999, Schultes et al. 2010, Dumont et al. 2011, Pearce et al. 2011), as well as by other factors such as species-dependent V_{diss} values (Kamatani 1982, Hurd & Birdwhistell 1983).

Importance of SAZ and PFZ in the global silicon budget

From a compilation of published results it appears that higher $bSiO_2$ production values in the SAZ and PFZ were more often observed in spring than in summer (Table 2). As expected, the PFZ was characterized by higher $bSiO_2$ production compared to the SAZ, resulting in greater PFZ seasonal $Si(OH)_4$ depletion by diatoms (<20 and <5 µmol l^{-1}, respectively) and a larger contribution of diatoms to primary production (Kopczynska et al. 2001, 2007, de Salas et al. 2011). The daily integrated $bSiO_2$ production in the SAZ (Table 2) was intermediate between the values reported for oligotrophic areas (0.1 to 2.9 mmol Si m^{-2}) and areas south of the Polar Front (1.8 to 93 mmol Si m^{-2}) (see review in Ragueneau et al. 2000, and subsequent studies by Brzezinski et al. 2001, Quéguiner 2001, Leblanc et al. 2002, Quéguiner & Brzezinski 2002, Beucher et al. 2004, Krause et al. 2009, 2010). The PFZ $bSiO_2$ production values were closer to the values reported south of the Polar Front.

Table 2. Mean and range of daily integrated $bSiO_2$ production and dissolution data and the dissolution to production (D:P) ratio for the euphotic layer in the Polar Frontal Zone (PFZ) and Subantarctic Zone (SAZ). Data from: Nelson & Gordon (1982), Caubert (1998), Brzezinski et al. (2001), Quéguiner (2001), Leblanc et al. (2002), Quéguiner & Brzezinski (2002), Beucher et al. (2004), present study

Zone	Season	$bSiO_2$ production (mmol m^{-2} d^{-1})		$bSiO_2$ dissolution (mmol m^{-2} d^{-1})		D:P	
		Mean	Range	Mean	Range	Mean	Range
SAZ	Spring	4.8 ± 4.7 (n = 7)	0.9–12.7	0.9 ± 0.7 (n = 5)	0.4–2.0	0.43 ± 0.22 (n = 5)	0.18–0.71
	Summer	1.1 ± 1.7 (n = 14)	0.1–6.6	2.7 ± 2.2 (n = 3)	0.9–5.2	1.74 ± 1.18 (n = 3)	1.0–3.1
PFZ	Spring	26.5 ± 16.3 (n = 13)	6.8–60.7	5.1 ± 1.0 (n = 2)	4.4–5.8	0.42 ± 0.28 (n = 2)	0.22–0.61
	Summer	3.0 ± 2.1 (n = 16)	0.3–9.1	4.5 ± 1.8 (n = 4)	2.2–6.5	1.70 ± 1.23 (n = 4)	0.73–3.50

Table 3. Annual gross and net $bSiO_2$ production for the spring and summer seasons by zone in the Polar Frontal Zone (PFZ) and Subantarctic Zone (SAZ). The mean values from Table 2 have been used for these estimations. Measurements were taken from October to March. Surface area: PFZ = 3×10^6 km^2: SAZ = 43.1×10^6 km^2 (JGOFS Synthesis Group 2001, Tomczak & Godfrey 1994)

Zone	Season	$bSiO_2$ gross production (mmol m^{-2} season^{-1})	$bSiO_2$ net production (mmol m^{-2} season^{-1})	$bSiO_2$ net production Tmol yr^{-1} zone^{-1}	% total zone^{-1}
SAZ	Spring	433 ± 423	246 ± 259	7.4 ± 13.2	4.3 ± 7.8
	Summer	101 ± 153	−75 ± 165		
	Spring + Summer	534 ± 449	171 ± 307		
PFZ	Spring	2382 ± 1467	1393 ± 1081	3.6 ± 3.3	2.1 ± 2.0
	Summer	271 ± 189	−190 ± 359		
	Spring + Summer	2653 ± 1479	1203 ± 1139		

For both the PFZ and SAZ, a net increase in the $bSiO_2$ pool has generally been observed in spring (mean D:P = 0.43 and 0.42, respectively), while in summer it is generally characterized by a net $bSiO_2$ loss (mean D:P = 1.74 and 1.70; Table 2). Brzezinski et al. (2003) suggested that a shift occurs from a condition in which $bSiO_2$ dissolution supports only a small fraction of the gross silica production that prevails during diatom blooms to a condition in which silica dissolution supports the major portion of the gross $bSiO_2$ production during non-bloom periods. With this scenario in mind, it would appear that during the SAZ-Sense study the second condition (non-bloom) prevailed both in the SAZ and PFZ. Our study suggests that the accumulation of dissolving detrital $bSiO_2$ following a diatom bloom can indeed sustain an efficient supply of Si through biologically mediated recycling in SAZ and PFZ surface waters.

Taking into account the mean integrated net $bSiO_2$ production for the spring and summer seasons (Table 3; October to March) and the PFZ and SAZ surface areas (JGOFS Synthesis Group 2001), we estimated the spring to summer net $bSiO_2$ production for the SAZ and PFZ to be 7.4 ± 13.2 and 3.6 ± 3.3 Tmol Si yr^{-1}, respectively. Tréguer & Van Bennekom (1991) estimated a PFZ gross $bSiO_2$ production at 2 Tmol Si yr^{-1}, significantly lower than our estimate (7.9 ± 4.4 Tmol Si yr^{-1}). They argued that their PFZ gross $bSiO_2$ production was probably underestimated since it was based on (lower) autumnal $bSiO_2$ production estimates. Using the early spring values of Nelson & Gordon (1982), Tréguer & Van Bennekom (1991) estimated a SAZ gross $bSiO_2$ production of 15.6 Tmol Si yr^{-1}, a value not very different from our estimate (23.0 ± 19.4 Tmol Si yr^{-1}). However, the dataset used in our study has been expanded considerably and is thus far more representative than the one utilized by Tréguer & Van Bennekom (1991). We also calculated that the SAZ and PFZ areas contributed to 4.3 ± 7.8 and 2.1 ± 2.0%, respectively, to the average global net $bSiO_2$ production of 171 ± 35 Tmol Si yr^{-1} (mean from Nelson et al. 1995, Usbeck 1999, Heinze et al. 2003, Jin et al. 2006). The PFZ has higher values by unit surface area, but the greater surface area of the SAZ explains its higher contribution to global $bSiO_2$ production (Table 3).

Si-dynamic at the deep PFZ $bSiO_2$ maximum

The subsurface chl *a* and $bSiO_2$ maxima at the base of the seasonal pycnocline have been a recurrent feature in the summer PFZ (Fig. 4b; Parslow et al. 2001, Quéguiner 2001, Bowie et al. 2011b). The origins of these deep maxima are unclear and vary according to location. Processes responsible for the formation of such features could be: (1) the development of an active community supported by a deep nutricline (Holm-Hansen & Hewes 2004), (2) the photophysiological acclimation of algal cells to low irradiance levels (Cullen 1982, Parslow et al. 2001), and (3) the sinking and accumulation of particles from the overlying mixed layer into a secondary pycnocline (Uitz et al. 2009).

C- and N-uptake rates in the deep $bSiO_2$ maximum decreased to minimal values, and production was mainly sustained by regenerated nutrients (Cavagna et al. 2011). There was no significant increase in the Si-uptake rate (Fig. 4d), and the large increase in the $bSiO_2$ D:P ratio at this depth also indicated efficient recycling of silicon. These observations argue against the development of an active community (see the first process possibility, above) but are more in favor of accumulation and recycling of both $bSiO_2$ and organic matter at the base of the seasonal pycnocline, just above the subsurface temperature minimum (100 to 250 m; Bowie et al. 2011b; the third process possibility).

CONCLUSIONS

The present study has significantly improved the quantification of the Si-budget in the euphotic layer for

the Southern Ocean SAZ and the PFZ regions. By compiling previous $bSiO_2$ production and dissolution data, a clear seasonal pattern emerges with (1) a higher production rate in spring than in summer and (2) a net gain of $bSiO_2$ production in the mixed layer in spring (D:P ratio ≈ 0.4), in contrast to a net loss in summer (D:P ratio ≈ 1.7). The PFZ has higher $bSiO_2$ production rates by unit surface area than the SAZ, in agreement with the higher diatom contributions to primary productivity there. We estimate the spring to summer net $bSiO_2$ production in the SAZ and the PFZ at 7.4 and 3.6 Tmol Si yr^{-1}, respectively, representing 4.3 and 2.1% of the global net $bSiO_2$ production (171 Tmol Si yr^{-1}).

Both in the late summer PFZ and SAZ, $bSiO_2$ dissolution is able to sustain the entire Si demand by diatoms. Such $bSiO_2$ dissolution suggests $bSiO_2$ accumulation within the mixed layer following upon bloom events. The SAZ environment appears to be characterized by more efficient dissolution (higher specific $bSiO_2$ dissolution rates) than the PFZ, likely induced by biological processes such as microzooplankton herbivory and bacterial activity, together with species-specific variation of V_{diss}.

Co-limitations (mainly iron) and the composition of diatom communities have been suggested as factors impacting Si-uptake kinetics and, consequently, the ability of diatoms to grow at low $Si(OH)_4$ concentrations. Specific Si-uptake rates (V_{Si}; d^{-1}) followed iron concentrations and were higher, intermediate, and lower in the eastern SAZ, western SAZ and PFZ, respectively.

At the deep $bSiO_2$ maximum in the PFZ we observed a decrease in gross primary production and an increase in the regenerated production for both Si and C. These observations argue against significant *in situ* growth of diatoms that are capable of extending productivity through easier access to deep, nutrient-rich pools. Instead our study provides evidence for the accumulation and recycling of settling detritic or living (partly inactive) cells at the base of the seasonal deep pycnocline (Bowie et al. 2011b).

Acknowledgements. Our warm thanks go to the officers and crew of RV 'Aurora Australis' during the SAZ-Sense cruise and also to B. Griffiths (chief scientist). We are also grateful to V. Barthaux (COM), J. Navez, L. Monin, and N. Dahkani (RMCA) for their help in sample processing and to I. Dumont (ULB) for bacterial activity measurements. This work was conducted within the BELCANTO III network (Contract SD/CA/03A of SPSDIII [Support Plan for Sustainable Development] funded by BELSPO [the Belgian Science Policy]) and within the EUR-OCEANS network of excellence (No. 511106, FP6, European Commission). L.A. acknowledges the support of Lotto and the FWO (Project FWONL36) in the acquisition of the HR-SF-ICP-MS. F.F. is a post-doctoral fellow of the 'Fonds de la Recherche Scientifique' (FNRS, Belgium), and D.C. was funded by BELSPO.

LITERATURE CITED

Armand LK, Cornet-Barthaux V, Mosseri J, Quéguiner B (2008) Late summer diatom biomass and community structure on and around the naturally iron-fertilized Kerguelen Plateau in the Southern Ocean. Deep-Sea Res II 55: 653–678

Beucher C, Tréguer P, Hapette AM, Corvaisier R, Pichon JJ (2004) Intense summer Si-recycling in the surface Southern Ocean. Geophys Res Lett 31:L09305. doi:10.1029/2003GL018998

Bidle KD, Azam F (1999) Accelerated dissolution of diatom silica by marine bacterial assemblages. Nature 397: 508–512

Bowie AR, Lannuzel D, Remenyi TA, Wagener T and others (2009) Biogeochemical iron budgets of the Southern Ocean south of Australia: summertime supply decouples iron and nutrient cycles in the subantarctic zone. Global Biogeochem Cycles 23:GB4034 doi:10.1029/2009GB003500

Bowie AR, Trull TW, Dehairs F (2011a) Editorial. Estimating the sensitivity of the Sub-Antarctic Zone to environmental change: The SAZ-Sense project. Deep-Sea Res II (in press) doi:10.1016/j.dsr2.2011.05.034

Bowie AR, Griffiths FB, Dehairs F, Trull TW (2011b) Oceanography of the sub-Antarctic and Polar Frontal Zones south of Australia during summer: setting for the SAZ-Sense study. Deep-Sea Res II (in press) doi:10.1016/j.dsr2.2011.05.033

Boyd PW, LaRoche J, Gall M, Frew R, McKay RML (1999) Role of iron, light, and silicate in controlling algal biomass in subantarctic waters SE of New Zealand. J Geophys Res 104:13395–13408

Brzezinski MA, Phillips DR, Chavez FP, Friederich GF, Dugdale RC (1997) Silica production in the Monterey, California, upwelling system. Limnol Oceanogr 42:1694–1705

Brzezinski MA, Nelson DM, Franck VM, Sigmon DE (2001) Silicon dynamics within an intense open-ocean diatom bloom in the Pacific sector of the Southern Ocean. Deep-Sea Res II 48:3997–4018

Brzezinski MA, Jones JL, Bidle KD, Azam F (2003) The balance between silica production and silica dissolution in the sea: insights from Monterey Bay, California, applied to the global data set. Limnol Oceanogr 48:1846–1854

Buesseler KO (1998) The decoupling of production and particulate export in the surface ocean. Global Biogeochem Cycles 12:297–310

Cardinal D, Alleman LY, Dehairs F, Savoye N, Trull TW, André L (2005) Relevance of silicon isotopes to Si-nutrient utilization and Si-source assessment in Antarctic waters. Global Biogeochem Cycles 19:GB2007. doi:10.1029/2004GB002364

Cassar N, DiFiore PJ, Barnett BA, Bender ML and others (2011) The influence of iron and light on net community production in the Subantarctic and Polar Frontal Zones. Biogeosciences 8:227–237

Caubert T (1998) Le cycle du silicium dans l'océan Austral: determination par spectrométrie de masse de la production de silice biogénique dans le secteur Indien. PhD thesis, Université de Bretagne Occidentale, Brest

Cavagna AJ, Elskens M, Griffiths FB, Fripiat F, Jacquet SHM, Dehairs F (2011) Contrasting regimes of productivity and potential for carbon export in the Subantarctic and Polar Frontal Zones south of Tasmania. Deep-Sea Res II (in press) doi:10.1016/j.dsr2.2011.05.026

Claquin P, Martin-Jézéquel V, Krompkamp JC, Veldhuis MJ, Kray GW (2002) Uncoupling of silicon compared to carbon

and nitrogen metabolisms and the role of the cell cycle in continuous cultures of *Thalassiosira pseudonana* (Bacillariophyceae) under light, nitrogen, and phosphorus control. J Phycol 38:922–930

Corvaisier R, Tréguer P, Beucher C, Elskens M (2005) Determination of the rate of production and dissolution of biosilica in marine waters by thermal ionisation mass spectrometry. Anal Chim Acta 534:149–155

Cullen JJ (1982) The deep chlorophyll maximum: comparing vertical profiles of chlorophyll *a*. Can J Fish Aquat Sci 39: 791–803

De La Rocha CL, Hutchins DA, Brzezinski MA, Zhang Y (2000) Effects of iron and zinc deficiency on elemental composition and silica production by diatoms. Mar Ecol Prog Ser 195:71–79

de Salas MF, Eriksen R, Davidson AT, Wright SW (2011) Protistan communities in the Australian sector of the Sub-Antarctic Zone during SAZ-Sense. Deep-Sea Res II (in press) doi:10.1016/j.dsr2.2011.05.032

Del Amo Y, Brzezinski MA (1999) The chemical form of dissolved Si taken up by marine diatoms. J Phycol 35: 1162–1170

Dumont I, Shoemann V, Jacquet SHM, Masson F, Becquevort S (2011) Bacterial abundance and production in epipelagic and mesopelagic waters in the Subantarctic and Polar Front zones south of Tasmania. Deep-Sea Res II (in press) doi:10.1016/j.dsr2.2011.05.024

Elskens M, de Brauwere A, Beucher C, Corvaisier R, Savoye N, Tréguer P, Baeyens W (2007) Statistical process control in assessing production and dissolution rates of biogenic silica in marine environments. Mar Chem 106:272–286

Franck VM, Brzezinski MA, Coale KH, Nelson DM (2000) Iron and silicic acid concentration regulate Si uptake north and south of the Polar Frontal Zone in the Pacific Sector of the Southern Ocean. Deep-Sea Res II 47:3315–3338

Franck VM, Bruland KW, Hutchins DA, Brzezinski MA (2003) Iron and zinc effects on silicic acid and nitrate uptake kinetics in three high-nutrient, low-chlorophyll (HNLC) regions. Mar Ecol Prog Ser 252:15–33

Fripiat F (2010) Isotopic approaches of the silicon cycle in the Southern Ocean. PhD thesis, Université Libre de Bruxelles, Brussels

Fripiat F, Corvaisier R, Navez J, Elskens M and others (2009) Measuring production–dissolution rates of marine biogenic silica by ^{30}Si-isotope dilution using a high-resolution sector field inductively coupled plasma mass spectrometer. Limnol Oceanogr Methods 7:470–478

Georg RB, Reynolds BC, Frank M, Halliday AN (2006) New sample preparation techniques for the determination of Si isotopic compositions using MC-ICPMS. Chem Geol 235: 95–104

Grasshoff K, Erhardt M, Kremling K (eds) (1983) Methods of seawater analysis, 2nd edn. Verlag Chemie, Weinheim

Heinze C, Hupe A, Maier-Reimer E, Diettert N, Ragueneau O (2003) Sensitivity of the marine biospheric Si cycle for biogeochemical parameter variations. Global Biogeochem Cycles 17(3):1086. doi:10.1029/2002GB001943

Herraiz-Borreguero L, Rintoul SR (2011) Regional circulation and its impact on upper ocean variability south of Tasmania. Deep-Sea Res II (in press) doi:10.1016/j.dsr2.2011.05.022

Hildebrand M (2008) Diatoms, biomineralization processes, and genomics. Chem Rev 108:4855–4874

Holm-Hansen O, Hewes CD (2004) Deep chlorophyll-*a* maxima (DCMs) in Antarctic waters. I. Relationships between DCMs and the physical, chemical, and optical conditions in the upper water column. Polar Biol 27:699–710

Hurd DC, Birdwhistell S (1983) On producing a general model for biogenic silica dissolution. Am J Sci 283:1–28

Hutchins DA, Sedwick PN, DiTullio GR, Boyd PW, Quéguiner B, Griffiths FB, Crossley C (2001) Control of phytoplankton growth by iron and silicic acid availability in the subantarctic Southern Ocean: experimental results from SAZ Project. J Geophys Res 106(C12):31559–31572

Jacquet SHM, Lam PJ, Trull T, Dehairs F (2011) Carbon export production in the subantarctic zone and polar front zone south of Tasmania. Deep-Sea Res II (in press) doi:10.1016/j.dsr2.2011.05.035

JGOFS Synthesis Group (Joint Ocean Global Flux Study Synthesis Group) (2001) Meeting of the Southern Ocean synthesis group, Year 1998. JGOFS Report 32

Jin X, Gruber JP, Sarmiento JL, Armstrong RA (2006) Diagnosing the contribution of phytoplankton functional groups to the production and export of particulate organic carbon, $CaCO_3$, and opal from global nutrient and alkalinity distributions. Global Biogeochem Cycles 20:GB2015. doi:10.1029/2005GB002532

Kamatani A (1982) Dissolution rates of silica from diatoms decomposing at various temperatures. Mar Biol 68:91–96

Karl DM, Tien G (1992) MAGIC: a sensitive and precise method for measuring dissolved phosphorus in aquatic environments. Limnol Oceanogr 37:105–106

Kopczynska EE, Dehairs F, Elskens M, Wright S (2001) Phytoplankton and microzooplankton variability between the Subtropical and Polar Fronts south of Australia: thriving under regenerative and new production in late summer. J Geophys Res 106(C12):31597–31609

Kopczynska EE, Savoye N, Dehairs F, Cardinal D, Elskens M (2007) Spring phytoplankton assemblages in the Southern Ocean between Australia and Antarctica. Polar Biol 31: 77–88

Krause JW, Nelson DM, Lomas MW (2009) Biogeochemical responses to late-winter storms in the Sargasso Sea, II: Increased rates of biogenic silica production and export. Deep-Sea Res I 56:861–874

Krause JW, Nelson DM, Lomas MW (2010) Production, dissolution, accumulation, and potential export of biogenic silica in a Sargasso Sea mode-water eddy. Limnol Oceanogr 55:569–579

Lannuzel D, Bowie AR, Remenyi T, Lam P and others (2011) Distributions of dissolved and particulate iron in the sub-Antarctic and Polar Frontal Southern Ocean (Australian sector). Deep-Sea Res II (in press) doi:10.1016/j.dsr2.2011.05.027

Leblanc K, Hutchins DA (2005) New applications of a biogenic silica deposition fluorophore in the study oceanic diatoms. Limnol Oceanogr Methods 3:462–476

Leblanc K, Quéguiner B, Fiala M, Blain S, Morvan J, Corvaisier R (2002) Particulate biogenic silica and carbon production rates and particulate matter distribution in the Indian sector of the Subantarctic Ocean. Deep-Sea Res II 49:3189–3206

Leynaert A, Bucciarelli E, Claquin P, Dugdale RC, Martin-Jézéquel V, Pondaven P, Ragueneau O (2004) Effect of iron deficiency on diatom cell size and silicic acid uptake kinetics. Limnol Oceanogr 49:1134–1143

Martin-Jézéquel V, Hildebrand M, Brzezinski MA (2000) Silicon metabolism in diatoms: implications for growth. J Phycol 36:821–840

Mongin M, Matear R, Chamberlain M (2011) Seasonal variability of remotely sensed chlorophyll and physical fields in the SAZ-Sense region. Deep-Sea Res II (in press) doi: 10.1016/j.dsr2.2011.06.002

Nelson DM, Goering JJ (1977a) A stable isotope tracer

method to measure silicic acid uptake by marine phytoplankton. Anal Biochem 78:139–147

Nelson DM, Goering JJ (1977b) Near-surface silica dissolution in the upwelling region off northwest Africa. Deep-Sea Res 24:65–73

Nelson DM, Gordon LI (1982) Production and pelagic dissolution of biogenic silica in the Southern Ocean. Geochim Cosmochim Acta 46:491–500

Nelson DM, Tréguer P, Brzezinski MA, Leynaert A, Quéguiner B (1995) Production and dissolution of biogenic silica in the ocean: revised global estimates, comparison with regional data and relationship to biogenic sedimentation. Global Biogeochem Cycles 9:359–372

Nelson DM, Brzezinski MA, Sigmon DE, Franck VM (2001) A seasonal progression of Si limitation in the Pacific sector of the Southern Ocean. Deep-Sea Res II 48:3973–3995

Parslow JS, Boyd PW, Rintoul SR, Griffiths FB (2001) A persistent subsurface chlorophyll maximum in the Interpolar Frontal Zone south of Australia: seasonal progression and implications for phytoplankton–light–nutrient interactions. J Geophys Res 106(C12):31543–31557

Pearce I, Davidson AT, Thomson PG, Wright S, van den Enden R (2011) Marine microbial ecology in the Sub-Antarctic Zone: rates of bacterial and phytoplankton growth and grazing by heterotrophic protists. Deep-Sea Res II (in press) doi:10.1016/j.dsr2.2011.05.030

Pondaven P, Ragueneau O, Tréguer P, Huvespre A, Dezileau L, Reyss JL (2000) Resolving the 'opal paradoxe' in the Southern Ocean. Nature 405:168–172

Quéguiner B (2001) Biogenic silica production in the Australian sector of the Subantarctic Zone of the Southern Ocean in late summer 1998. J Geophys Res 106(C12):31627–31636

Quéguiner B, Brzezinski MA (2002) Biogenic silica production rates and particulate matter distribution in the Atlantic sector of the Southern Ocean during austral spring 1992. Deep-Sea Res II 49:1765–1786

Ragueneau O, Tréguer P, Leynaert A, Anderson RF and others (2000) A review of the Si cycle in the modern ocean: recent progress and missing gaps in the application of biogenic opal as a paleoproductivity proxy. Global Planet Change 26:317–365

Ragueneau O, Savoye N, Del Amo Y, Cotten J, Tardiveau B, Leynaert A (2005) A new method for the measurement of biogenic silica in suspended matter of coastal waters: using Si:Al ratios to correct for the mineral interference. Cont Shelf Res 25:697–710

Rintoul SR, Bullister JL (1999) A late winter hydrographic section from Tasmania to Antarctica. Deep-Sea Res I 46: 1417–1454

Sarmiento JL, Gruber N, Brzezinski MA, Dunne JP (2004) High-latitude controls of thermocline nutrients and low latitude biological productivity. Nature 427:56–60

Sarthou G, Timmermans KR, Blain S, Tréguer P (2005) Growth physiology and fate of diatoms in the ocean: a review. J Sea Res 53:25–42

Schultes S, Lambert C, Pondaven P, Corvaisier R, Jansen S, Ragueneau O (2010) Recycling and uptake of $Si(OH)_4$ when protozoan grazers feed on diatoms. Protist 161:288–303

Sedwick PN, Blain S, Quéguiner B, Griffiths FB, Fiala M, Bucciarelli E, Denis M (2002) Resource limitation of phytoplankton growth in the Crozet Basin, SubAntarctic Southern Ocean. Deep-Sea Res II 49:3327–3349

Sigman DM, Hain MP, Haug GH (2010) The polar ocean and glacial cycles in atmospheric CO_2 concentration. Nature 466:47–55

Takeda S (1998) Influence of iron availability on nutrient consumption ratio of diatoms in oceanic waters. Nature 393: 774–777

Thamatrakoln K, Hildebrand M (2008) Silicon uptake in diatoms revisited: a model for saturable and nonsaturable uptake kinetics and the role of silicon transporters. Plant Physiol 146:1397–1407

Tomczak M, Godfrey JS (1994) Antarctic oceanography. In: Tomczak M, Godgrey JS (eds) Regional Oceanography: An Introduction. Pergamon, New York, NY, p 63–82

Tréguer P, Van Bennekom AJ (1991) The annual production of biogenic silica in the Antarctic Ocean. Mar Chem 35: 477–487

Tréguer P, Lindner L, van Bennekom AJ, Leynaert A, Panouse M, Jacques G (1991) Production of biogenic silica in the Weddell–Scotia Seas measured with ^{32}Si. Limnol Oceanogr 36:1217–1227

Tréguer P, Nelson DM, van Bennekom AJ, DeMaster DJ, Leynaert A, Quéguiner B (1995) The silica balance in the world ocean: a re-estimate. Science 268:375–379

Uitz J, Claustre H, Griffiths FB, Ras J, Garcia N, Sandroni V (2009) A phytoplankton class-specific primary production model applied to the Kerguelen Islands region (Southern Ocean). Deep-Sea Res I 56:541–560

Usbeck R (1999) Modeling of marine biogeochemical cycles with an emphasis on vertical particle fluxes. PhD thesis, University of Bremen

Editorial responsibility: Katherine Richardson, Copenhagen, Denmark

Submitted: September 8, 2010; Accepted: June 1, 2011
Proofs received from author(s): August 12, 2011